

Journal of Materials Chemistry A

Accepted Manuscript



This is an *Accepted Manuscript*, which has been through the Royal Society of Chemistry peer review process and has been accepted for publication.

Accepted Manuscripts are published online shortly after acceptance, before technical editing, formatting and proof reading. Using this free service, authors can make their results available to the community, in citable form, before we publish the edited article. We will replace this *Accepted Manuscript* with the edited and formatted *Advance Article* as soon as it is available.

You can find more information about *Accepted Manuscripts* in the [Information for Authors](#).

Please note that technical editing may introduce minor changes to the text and/or graphics, which may alter content. The journal's standard [Terms & Conditions](#) and the [Ethical guidelines](#) still apply. In no event shall the Royal Society of Chemistry be held responsible for any errors or omissions in this *Accepted Manuscript* or any consequences arising from the use of any information it contains.



Journal Name

ARTICLE

Si nanoparticles adhering to the nitrogen-rich porous carbon framework and their application as lithium-ion battery anode materials

Received 00th January 20xx,
Accepted 00th January 20xx

DOI: 10.1039/x0xx00000x

www.rsc.org/

Lu Shi,^{abc} Weikun Wang,^{*c} Anbang Wang,^{*c} Keguo Yuan,^c Zhaoqing Jin^c and Yusheng Yang^c

In this work, a novel Si/nitrogen-rich porous C composite was prepared by the simple co-assembly of gelatin, nano-CaCO₃ particles and Si nanoparticles, followed by a pyrolysis process and a subsequent acid washing treatment to remove the template. The Si nanoparticles were adhering to the nitrogen-rich porous carbon framework, which possesses good conductivity and adequate free space to accommodate the volume change of Si nanoparticles during cycling. By contrast with the bare Si nanoparticles and the conventional Si/C composite, the electrochemical performance of the as-prepared Si/nitrogen-rich porous C composite has been improved significantly. It delivers a reversible capacity of 1103 mA h g⁻¹ after 100 cycles at a current density of 100 mA g⁻¹ and 766 mA h g⁻¹ at 2 A g⁻¹, much higher than those of commercial graphite anodes. In addition, the synthesis method can be easily scaled up and widely applied to other high-capacity anode and cathode materials systems that undergo large volume expansion.

Introduction

The rapid development of portable electronic devices, electric vehicles and grid storage has brought increasing demand for the high-performance lithium-ion batteries with light weight, high energy density, long cycle life and high rate performance.^{1,2} However, the limited theoretical capacity (372 mA h g⁻¹) of the graphite anodes used in the currently commercial Li-ion batteries can not satisfy the demand of high energy density. Hence, developing a low-cost electrode material with high energy capacity via a simple method can lead to a significant improvement in high performance lithium-ion batteries. Among the various anode materials, silicon has been regarded as one of the most promising candidates to replace the conventional graphite anodes, due to its much higher theoretical specific capacity (about 4200 mA h g⁻¹), moderate working potential (<0.5 V vs. Li/Li⁺) and the high resource abundance.^{3,4} However, the large-scale application of silicon has been seriously hampered by the low intrinsic electric conductivity and large volume changes (up to 400%)

during the lithium insertion and extraction processes. The huge volume changes can cause pulverization and loss of electrical contact between Si particles and conductive additives, as well as an unstable solid electrolyte interphase (SEI) layer, resulting in severe capacity fading.^{4,5}

Accordingly, to address these above issues and improve the electrochemical performance of silicon-based lithium-ion battery anodes, many studies have been conducted to design different nanostructured forms of Si, such as silicon nanowires,⁶⁻⁸ silicon nanotubes,⁹⁻¹¹ silicon nanofibers,^{12,13} silicon hollow nanospheres,¹⁴ nanoscale thin films^{15,16} and porous silicon.^{17,18} Meanwhile, these different nanostructured forms of Si are always combined with carbon materials (or graphene) to further enhance the electrochemical performance. The Si nanoparticles are also combined with the carbon materials to fabricate the Si/C composites with different structures, such as the core-shell structure,¹⁹ the hollow core-shell structure²⁰ and the three-dimensional porous structure.²¹ In particular, the combination of carbon materials with the Si anodes has been recognized as an efficient approach to improve the cycling performance, as the carbon component can not only improve the electric conductivity of the Si anodes but also play a structural buffering role to accommodate the volume change of Si and minimize the mechanical stress, thus preventing the deterioration of the electrode integrity. However, the volume swelling and mechanical pulverization of these conventional Si/C composites are still difficult to be avoided due to the absence of abundant internal free space to accommodate the severe volume changes of Si during its alloying/dealloying processes.^{22,23}

The porous carbon materials, which possess high specific surface area, large porosity, excellent conductivity, high

^a College of Chemistry and Chemical Engineering, Xinxiang University, Henan Xinxiang 453000, China. E-mail: lulus1987@163.com

^b School of Materials Science & Engineering, Beijing Institute of Technology, Beijing 100081, China

^c Military Power Sources Research and Development Center, Research Institute of Chemical Defense, Beijing 100191, China. E-mail: wangweikun2002@163.com; wab_wang2000@aliyun.com; Fax: +86-10-66748499; Tel: +86-10-66705840

† Electronic Supplementary Information (ESI) available: SEM image of the Si/porous C composite and its corresponding EDS mapping images; TEM image of the nano-CaCO₃ particles; Pore size distribution of the Si/porous C composite; Raman spectra of the Si, porous C, Si/C and Si/porous C composites; Cycling performance of the Si nanoparticles before and after HF solution cleaning. See DOI: 10.1039/x0xx00000x

resiliency and good mechanical strength, is regarded as an ideal buffering matrix for Si nanoparticles to efficiently alleviate their volume change.²⁴ Therefore, in this work, we adhere the Si nanoparticles to the nitrogen-rich porous carbon framework and construct the Si/nitrogen-rich porous C composite by a very simple method. The nitrogen-rich porous carbon matrix is prepared by pyrolyzing the cheap and environmentally friendly gelatin and using the nano-CaCO₃ particles as template. After the pyrolysis of gelatin, the nitrogen atoms exist in the carbon material in the form of pyridinic nitrogen, pyrrolic nitrogen, pyridonic nitrogen and graphitic nitrogen and it is believed that the nitrogen-rich carbon materials play a positive role for lithium insertion due to the stronger interaction between the nitrogen-rich carbon materials and lithium.^{25,26} In addition, incorporation of Nitrogen into the carbon materials may introduce the vacancies and dangling bonds around the nitrogen sites, which may enhance the Li storage capacity.¹⁹ With the Si nanoparticles adhering to the nitrogen-rich porous carbon framework, enough space can be reserved to effectively accommodate its volume change, thus enhancing its cycling stability. Especially, this structure can be easily produced on a large scale with a controllable approach at low cost and this successful material design could also be extended to other high-capacity anode and cathode materials systems that undergo large volume expansion.

Experimental

Sample preparation

Fig. 1 gives an overview of the synthetic process of the Si/nitrogen-rich porous C composite, named as Si/porous C. The synthetic process is very simple and can be divided into the following three steps. Firstly, the Si nanoparticles (ca. 200 nm; Xuzhou Lingyun Silicon Industry Co., Ltd), CaCO₃ nanoparticles (ca. 50 nm; Shanxi Xintai NanoMater. Co., Ltd) were added into a gelatin aqueous solution, and then the mixture was stirred at room temperature to obtain a homogeneous solution. The Si nanoparticles, nano-CaCO₃ particles and gelatin were prepared in the weight ratio of 1:1:1. The solution was dried at 60 °C while being mechanically stirred to insure a homogeneous distribution of nano-Si and nano-CaCO₃ particles in the gelatin matrix. The CaCO₃ nanoparticles were used as the template and commercial gelatin as the carbon precursor. Secondly, the mixture was carbonized at 800 °C in nitrogen (99.999%) for 3 h at a heating rate of 5 °C min⁻¹. Finally, the obtained mixture was dispersed in 30 wt% HCl solution to remove the hard template and then was immersed into 5 wt% HF solution to remove the SiO₂ formed during the synthetic process. Pure porous carbon

without Si nanoparticles and the Si/C composite without using the template nano-CaCO₃ particles were also synthesized using the same procedure described above.

Structural characterization

The microstructures of the samples were examined by scanning electron microscopy (SEM) (JSM-5600LV, JEOL, Tokyo, Japan) and transmission electron microscopy (TEM) (JEM-2010F, JEOL, Tokyo, Japan). Nitrogen adsorption-desorption isotherms of the composites were measured at 77 K with a NOVA1200 instrument (Quantachrome Corporation). Total specific area was determined by multipoint Braunauer-Emmett-Teller method. The BJH pore size distribution was calculated based on the desorption branch of the isotherm. The amount of carbon in the composites was determined by thermogravimetric (TG) analysis using a Perkin-Elmer TGA 7 thermogravimetric analyzer from 40 °C to 1000 °C with a heating rate of 10 °C min⁻¹ in air. The phase composition of the samples were determined by a Rigaku B/max-2400X with Cu K α radiation in the 2 θ range of 10° to 90°. Raman spectroscopy (Renishaw in Viacmicro-Raman spectroscopy system equipped with a 514.5 nm laser) was used to investigate the existence of carbon of the composites. X-ray photoelectron spectra (XPS) were recorded on an AXIS Ultra DLD spectrometer (Kratos) to characterize the surface composition.

Electrochemical measurements

Electrochemical experiments were performed using CR2025-type coin cells assembled in an argon-filled glove box with Celgard 2400 membrane as separator and lithium-foil as counter electrode. The electrolyte employed was 1M LiPF₆ in the mixture of ethylene carbonate (EC) and dimethyl carbonate (DMC) (1:1 in volume ratio) containing 2 wt% vinylene carbonate (VC) as additive. The working electrode was prepared by casting a mixture of 60 wt% active material, 20 wt% acetylene black and 20 wt% sodium alginate dissolved in deionized water on a copper current collector. The active materials mass loading was approximately 1 mg cm⁻². Prior to cell fabrication, the electrodes were degassed in vacuum oven at 120 °C for at least 6 h. The electrochemical performances were evaluated on a LAND CT2001A multi-channel battery test system at room temperature. If not mentioned otherwise, the galvanostatic voltage cutoffs were 0.01 and 1.5 V vs Li/Li⁺. Cyclic voltammetry (CV) measurement was performed on a CHI660D electrochemical workstation at a scan rate of 0.1 mV s⁻¹. Electrochemical impedance spectroscopy (EIS) was also carried out on this instrument in the frequency range from 10⁵ to 0.01 Hz and the amplitude of the used perturbation was 10 mV. The specific capacity was calculated based on the total mass of the active material.

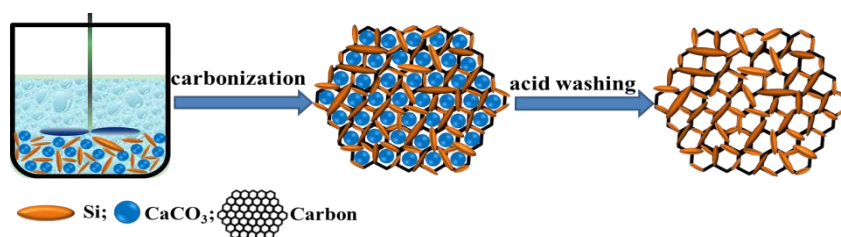


Fig. 1 Schematic illustration of the synthesis of the silicon/nitrogen-rich porous carbon composite.

Results and discussion

Fig. 2 shows the SEM images of the pure porous carbon, Si, Si/C and Si/porous C composites. The well-developed interconnected pore structure with abundant porous channels is observed in the porous carbon (Fig. 2a). From Fig. 2b, it can be seen that the pristine silicon particles are connected and agglomerated to some extent. However, the Si/C composite (Fig. 2c) displays the entirely different morphology from the pristine silicon. The size of the particles becomes larger after the carbon coating. The SEM image of the Si/porous C composite in Fig. 2d clearly shows that the Si nanoparticles are distributed evenly and adhering to the porous carbon framework, which is further confirmed by its elemental mapping images in Fig. S2.

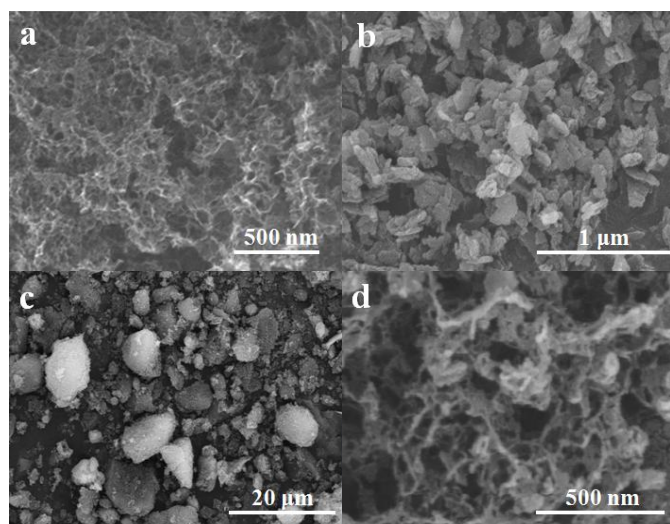


Fig. 2 SEM images of the porous C (a), Si (b), Si/C (c) and Si/porous C composites (d).

Fig. 3 presents the TEM images of the as-prepared samples. The porous C (Fig. 3a) shows rich pore structure with the pore size of about 50 nm, close to the diameter of nano-CaCO₃ particles (Fig. S3). What's more, as shown from its HRTEM image (Fig. 3a insert), it exhibits a disordered turbostratic graphite structure. The Si nanoparticles show the irregularly rod-like morphology, each about 30 nm in diameter and 200 nm in length. Its HRTEM (Fig. 3b insert) shows the interplanar spacing of Si, which is consistent with the (111) planes. Besides, it can be seen that the Si nanoparticles are coated with a thin layer of amorphous microstructure which may refer to the SiO₂ layer as silicon nanoparticles are easily oxidized. The TEM image of the Si/C composite (Fig. 3c) shows a uniform distribution of Si nanoparticles in the carbon matrix. Fig. 3d shows the TEM image of the as-prepared Si/porous C sample. It clearly indicates that the Si nanoparticles are adhering to the porous carbon framework and distributed uniformly. Its HRTEM (Fig. 3d insert) further corroborates the homodisperse of nano-silicon in the amorphous microstructure of porous carbon matrix. The porous carbon matrix not only provides an efficient electron transportation network, but also acts as a strain absorb which can offer a flexible mechanical support for the expansion and contraction of Si nanoparticles during the lithiation/delithiation process.

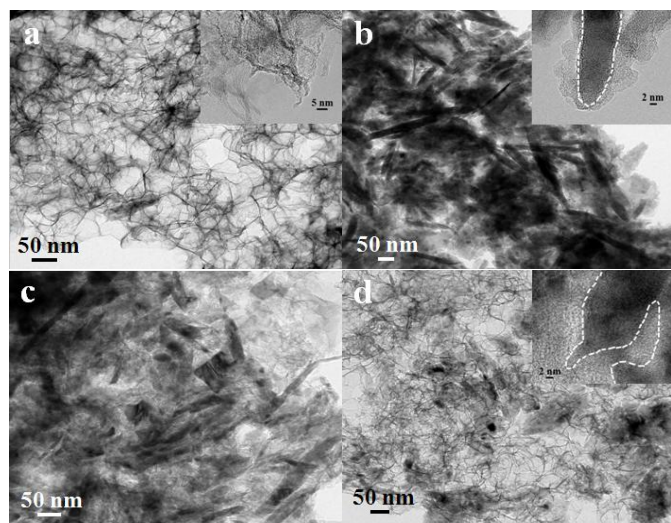


Fig. 3 TEM images of the porous C (a), Si (b), Si/C (c) and Si/porous C composite (d).

The pore structure of the samples was further investigated by the nitrogen adsorption-desorption isotherms measurements. The Brunauer-Emmett-Teller (BET) specific surface and pore volume of the Si nanoparticles are $155 \text{ m}^2 \text{ g}^{-1}$ and $0.42 \text{ cm}^3 \text{ g}^{-1}$, respectively. The nitrogen adsorption-desorption isotherms of the porous C (Fig. 4a) show a type-IV curve with distinct hysteresis loop at high relative pressures, typical of mesoporous materials. It shows a BET surface area of $641 \text{ m}^2 \text{ g}^{-1}$ and a pore volume of $1.51 \text{ cm}^3 \text{ g}^{-1}$. The pore diameter distributions determined by the Barrett-Joyner-Halenda (BJH) analysis indicate the pore diameter of the porous C lies in the size range of 40-50 nm (Fig. 4b), which is close to the particle size of the CaCO_3 nanoparticles and in line with the former TEM results. After dispersing the Si nanoparticles into the carbon matrix without the porous structure, the obtained Si/C composite shows a BET surface area of $199 \text{ m}^2 \text{ g}^{-1}$ and a pore volume of $0.63 \text{ m}^3 \text{ g}^{-1}$. Compared with the Si nanoparticles, the increased BET surface area of the Si/C composite is attributed to the carbon matrix. After the Si nanoparticles adhering to the porous carbon framework, the specific surface area of the Si/porous C composite decreases from $641 \text{ m}^2 \text{ g}^{-1}$ to $252 \text{ m}^2 \text{ g}^{-1}$ and the pore volume reduces from $1.51 \text{ cm}^3 \text{ g}^{-1}$ to $0.78 \text{ cm}^3 \text{ g}^{-1}$. As shown in Fig. S4, its pore diameter lies in the size range of 40-60 nm, consistent with that of the porous C. The highly-developed porous structure of the Si/porous C composite can not only accommodate the volume change of Si nanoparticles during the charging/discharging process but also can facilitate the Li^+ ion transport and improve the electrochemical reaction kinetics.

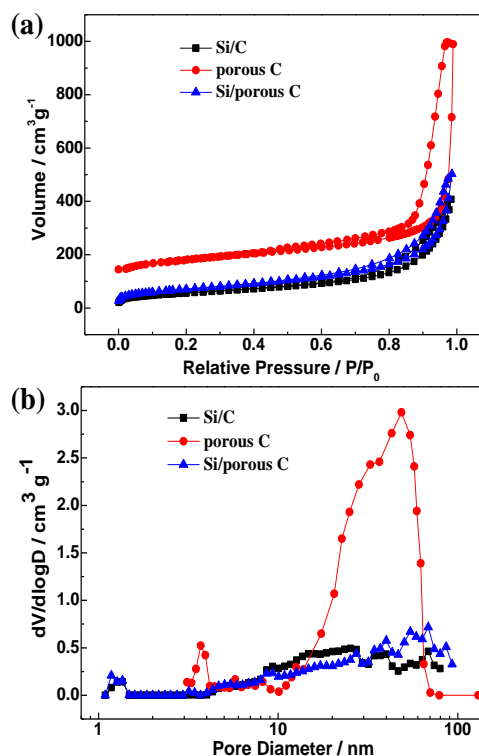


Fig. 4 (a) Nitrogen adsorption-desorption isotherms and (b) the pore size distribution of porous C, Si/C and Si/porous C composites.

Fig. 5 presents the thermogravimetric (TG) analysis curves of the porous C, Si/C and Si/porous C composites from 40°C to 1000°C in air. The weight losses occurring in the temperature range of 400°C to 800°C for the Si/C and Si/porous C composites correspond to the oxidation of the carbon. When the temperature is higher than 800°C , the carbon is completely combusted. Therefore, the carbon contents determined by the TG analysis are estimated to be 40 wt% and 44 wt% for the Si/C and Si/porous C composites. The weight percent of Si in Si/C and Si/porous C composites is calculated to be 60 wt% and 56 wt%, respectively. The weight increase at the temperature above 800°C is ascribed to the oxidation of silicon into SiO_x in the Si/C and Si/porous C composites.^{24,27}

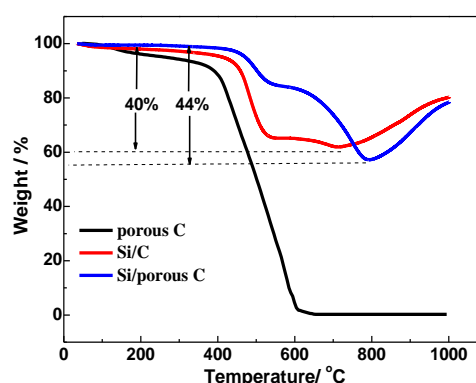


Fig. 5 TG curves of the porous C, Si/C and Si/porous C composites under air atmosphere from 40°C to 1000°C .

Fig. 6 presents the XRD patterns of the porous C, Si, Si/C and Si/porous C composites. For porous C, two broad diffraction

peaks at 2θ of 23° and 43° can be assigned to the (002) and (100) planes of carbon, indicating a non-graphitized structure.^{28,29} For the Si, Si/C and Si/porous C composites, the intensive well-defined peaks at 2θ of 28.4° , 47.4° , 56.2° , 69.2° and 76.5° can be indexed as the (111), (220), (311), (400) and (331) planes of Si crystals,¹⁸ respectively. What's more, after the carbonization process, the diffraction peaks of Si for the Si/C and Si/porous C composites do not change significantly, indicating that the crystal structure of Si in the composites remain intact. Besides, the Raman spectra (Fig. S5) further confirm the presence of Si and amorphous carbon in the Si/C and Si/porous C composites.³⁰⁻³²

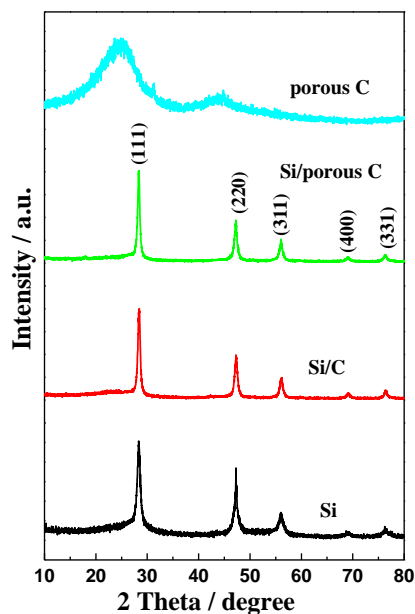


Fig. 6 XRD patterns of the porous C, Si, Si/C and Si/porous C composites.

Fig. 7a displays the wide scan XPS spectra of the Si nanoparticles and Si/porous C composite, showing the major peaks which are due to silicon (Si 2p), nitrogen (N 1s), oxygen (O 1s) and carbon (C 1s). All of the peaks are classified according to their binding energy. Compared with the Si nanoparticles, the weaker Si 2p peak at 100.4 eV for the Si/porous C composite suggests that the Si nanoparticles are well adhering to the porous carbon framework. The stronger C 1s peak at 284.0 eV for the Si/porous C composite may arise from the carbon pyrolysed from gelatin. The stronger O 1s peak at 530.0 eV for the Si nanoparticles is due to the oxidation of the surface of Si nanoparticles. For the Si/porous C composite, a relatively weaker O 1s peak is observed, further demonstrating that the Si nanoparticles are well dispersed in the porous carbon framework. What's more, by contrast with the Si nanoparticles, the Si/porous C composite shows the obvious N 1s peak at 400.0 eV, indicating that the porous carbon framework is rich in nitrogen. The N content in the Si/porous C composite is about 2.5 wt%. And dispersing the Si nanoparticles in the nitrogen-rich carbon is believed to be beneficial for lithium insertion.^{33,34} The formation of vacancies and dangling bonds around the nitrogen sites may enhance the reactivity and the electronic conductivity of N-doped carbon, which could play a positive effect on the electrochemical performance of the Si/porous C composite as anode material

for lithium-ion batteries.¹⁹ Furthermore, as shown in Fig. 7b, the N1s spectrum can be divided into 397.8, 399.8, 403.5 eV, corresponding to pyridinic, pyrrolic/pyridonic and graphitic nitrogen atoms, respectively, according to Kapteijn's assignments.³⁵

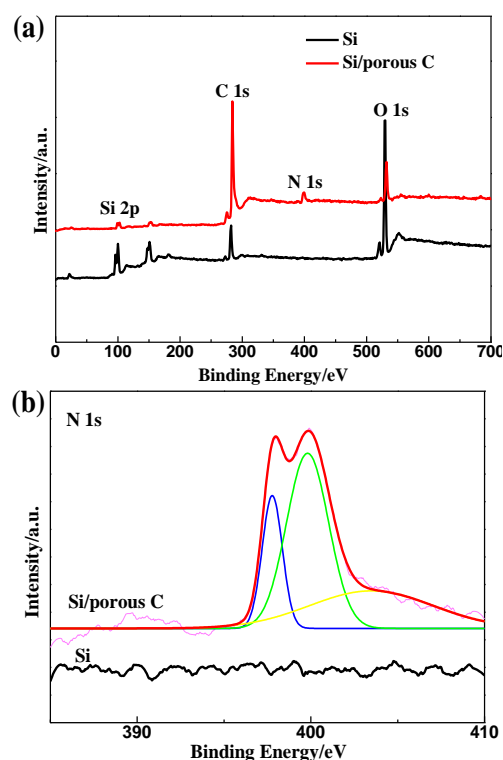


Fig. 7 XPS spectra of the Si and Si/porous C composite (a) wide spectra; (b) N1s.

The Si and the as-prepared samples are employed as electrode materials to evaluate the electrochemical properties. Fig. 8a exhibits the cyclic voltammetry (CV) curves in the initial three cycles of the Si/porous C electrode at the scan rate of 0.1 mV s^{-1} . During the first cathodic scanning cycle, the small reduction peak located at around 1.2 V may be ascribed to the formation of the SEI film,³⁶ which disappears from the second cycle, reflecting the stable character of SEI film formed at the first cycle. The peak at 0.01 V corresponds to the Li-insertion process of crystalline Si to form the amorphous Li_xSi phase. In the anodic scanning cycle, two peaks located at 0.3 V and 0.5 V are attributed to the phase transition between amorphous Li_xSi and amorphous silicon. After the first cycle, the scans show a repeatable shape. The CV curve area is increasing in the subsequent cycles, which is due to the initial activation of the electrode material, enabling more Li to alloy with Si.³⁷⁻³⁹

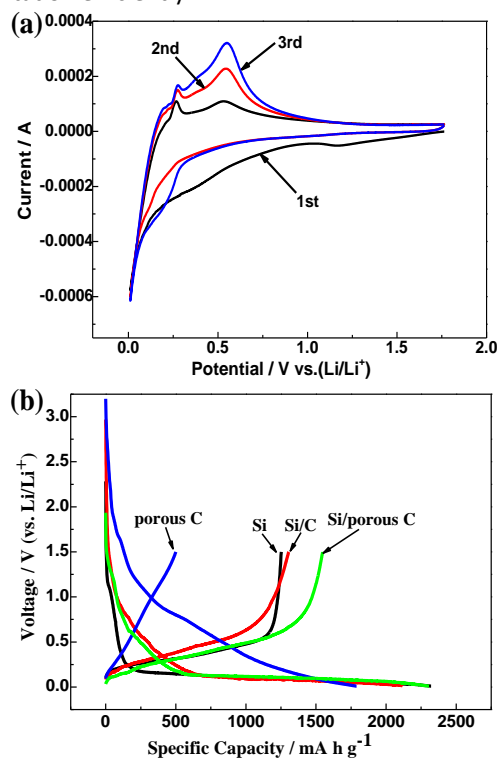
Fig. 8b shows the charge/discharge profiles of the porous C, Si, Si/C and Si/porous C composites in the voltage window of 0.01-1.5 V at a current density of 100 mA g^{-1} in the first cycle. During the first cycle discharge, the slope potential of the Si/C and Si/porous C anodes decrease in the high potential area is mainly attributed to the lithiation of the carbon, while the long flat plateau below 0.1 V is ascribed to the typical lithiation process of crystalline Si to form amorphous Li_xSi phase. During the first cycle charge, the voltage plateau of the Si, Si/C and Si/porous C anodes at 0.4 V corresponds to the de-alloying process of Li_xSi . The Si nanoparticles deliver an initial specific

discharge and charge capacity of 2320 and 1252 mA h g⁻¹ with an initial coulombic efficiency of 54%, while the porous C shows an initial specific discharge capacity of 1790 mA h g⁻¹ and a specific charge capacity of 500 mA h g⁻¹, with an initial coulombic efficiency of 28%. After dispersing the Si nanoparticles into the carbon matrix, the obtained Si/C composite shows the first cycle specific discharge capacity of 2119 mA h g⁻¹ and the first cycle specific charge capacity of 1305 mA h g⁻¹, with the initial coulombic efficiency of 62%. Then after adhering the silicon nanoparticles to the nitrogen-rich porous carbon framework, the obtained Si/porous C composite delivers an initial specific discharge and charge capacity of 2306 and 1548 mA h g⁻¹ with an initial coulombic efficiency of 67%. The lower initial specific discharge capacity and the coulombic efficiency of the Si nanoparticles may be attributed to the oxide layer of SiO₂ formed on the surface of the Si nanoparticles, the dead Li which was not dealloyed during the charge process because of the pulverization of the electrode from the huge volume change and the solid-electrolyte interface (SEI) layer formation on the surface of the electrode. The low initial coulombic efficiency of the porous C is supposed to originate from the SEI layer formation on the surface of the porous C with larger specific surface areas, consuming more lithium. Meanwhile, the irreversible lithium intercalation due to the residual electrochemically active surface groups such as C-H in the low-temperature pyrolyzed carbon materials may also bring down its initial coulombic efficiency.⁴⁰ The huge initial irreversible capacity of the Si/C and Si/porous C composites may be mainly attributed to the reasons mentioned above.

Fig. 8c demonstrates the cycling performance of the porous C, Si, Si/C and Si/porous C composites at a current density of 100 mA g⁻¹. The capacity of the bare Si nanoparticles drops quickly to 80 mA h g⁻¹ after 100 cycles. Even if precleaned by HF solution to remove the surface oxides, the Si nanoparticles still reveal a fast capacity fading (Fig. S6). The rapid capacity loss is attributed to the particle pulverization and the poor electrical contact of the electrode from the current collector resulting from the large volume change during the cycling. For comparison, the bare porous C derived from gelatin shows a stable but relatively low capacity of about 360 mA h g⁻¹. Then after dispersing the Si nanoparticles into the nitrogen-rich carbon matrix, the cycling performance of the obtained Si/C composite has been improved a lot by contrast with the pure Si nanoparticles. However, it still delivers an obvious capacity fading and maintains a reversible capacity of 404 mA h g⁻¹ after 100 cycles with a capacity retention of about 30 % as against the second cycle. The rapid capacity fading of the Si/C composite is due to the nitrogen-rich carbon matrix with nonporous structure which cannot effectively buffer the large volume change of Si nanoparticles during the Li-ion insertion/extraction process. Finally, after the Si nanoparticles are adhering to the nitrogen-rich porous carbon framework, the cycling performance of the as-prepared Si/porous C composite has been significantly improved. It delivers the highest reversible capacity of 1103 mA h g⁻¹ and excellent cycle stability with the capacity retention of 72% as against the

second cycle after 100 cycles, which is three times higher than that of graphite. Moreover, its coulombic efficiency reaches approximate 99% in 100 cycles. Compared with other nitrogen containing Si/C composites, the Si/porous C composite still has certain advantages in terms of its electrochemical performance. The N-containing core-shell Si/C nanocomposite prepared by carbonization of polyaniline exhibits the specific capacity of 795 mA h g⁻¹ after 50 cycles at 100 mA g⁻¹.¹⁹ The good cycling performance of the Si/porous C composite can be ascribed to the nitrogen-rich porous carbon framework which serves as an electrochemically stable buffer matrix and can afford enough space for the large volume change of Si nanoparticles in the lithiation/delithiation process. Therefore, the stable structure of the Si/nitrogen-rich porous C composite can keep tight contact of active materials with the electrode framework and hence avoid electrode from pulverization.

Fig. 8d shows the rate performance of the Si/porous C composite. It delivers the reversible capacities of 1430, 1285, 1175, 1018, 912 mA h g⁻¹ at a current density of 100, 200, 400, 800 and 1000 mA g⁻¹, respectively. Even at a higher current density of 2000 mA g⁻¹, a stable reversible capacity of 766 mA h g⁻¹ could be obtained, showing a good rate performance. Notably, the reversible capacity can recover to about 1174 mA h g⁻¹ once the current density goes back to 100 mA g⁻¹, indicating that the Si/porous C composite exhibits a good electrochemical reversibility and structural integrity.^{41,42} Moreover, the charge/discharge curves at different rates have also been presented to exhibit the rate behaviors of the Si/porous C composite (Fig. S7). The satisfying rate performance of the Si/porous C composite is ascribed to the highly-developed porous structure of the nitrogen-rich carbon framework which can facilitate the electronic and ionic transportation efficiently.



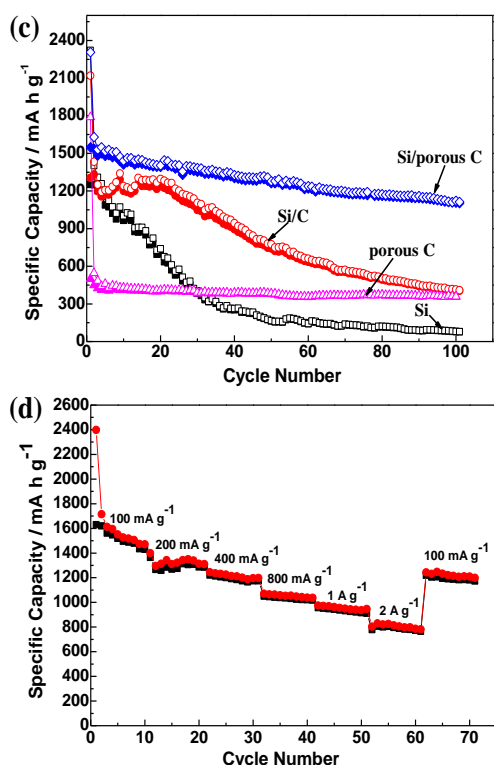


Fig. 8 (a) Cyclic voltammogram curves of the Si/porous C electrode from the first cycle to the third cycle at a scan rate of 0.1 mV s^{-1} ; (b) The first cycle charge-discharge curves of the porous C, Si, Si/C and Si/porous C composites at 100 mA g^{-1} in the voltage window of $0.01\text{-}1.5 \text{ V}$; (c) The cycling performance of the porous C, Si, Si/C and Si/porous C composites at 100 mA g^{-1} ; (d) The rate performance of the Si/porous C composite at various current densities.

Fig. 9 presents the surface morphology of the electrodes of Si, Si/C and Si/porous C before and after 100 cycles. The three kinds of electrodes show almost the same morphology before cycling, just as shown in Fig. 9a, Fig. 9c and Fig. 9e for the Si electrode, Si/C electrode and Si/porous C electrode, respectively. However, after 100 cycles, the structural differences between the electrodes can be clearly distinguished. The Si electrode (Fig. 9b) and Si/C electrode (Fig. 9d) crack as a result of the large volume expansion and contraction of the Si nanoparticles during the cycling. The pulverization of the two electrodes is obvious, especially for the Si electrode. As a comparison, the Si/porous C electrode (Fig. 9f) still maintains its integrity and contains no larger cracks after 100 cycles, further confirming its stable structure. The well-developed porous structure of the nitrogen-rich porous carbon matrix which acts as a stress reliever during the expansion and contraction of silicon nanoparticles prevents the cracks and eventual pulverization of the electrode, thus improving the capacity and the cycle life.

To further compare the electrochemical reaction kinetics of the bare Si, Si/C and Si/porous C anodes, the electrochemical impedance spectroscopy (EIS) was recorded from 10^5 to 0.01 Hz before cycling and after 100 cycles. As shown in Fig. 10, all of them consist of a depressed semicircle in the high frequency region and a sloping line in the low frequency domain. The depressed semicircles in the high frequency region correspond to the interface impedance, which is associated with the resistance of the SEI film (R_f) and the charge-transfer

resistance of Li-ion insertion (R_{ct}).⁴³ The inclined low frequency line corresponds to lithium-ion diffusion impedance.⁴⁴ According to the Nyquist plots before cycling, the relatively smaller radius of the semicircles for Si/C and Si/porous C electrodes represent a lower electrochemical interface impedance than that of the bare nano-Si electrode, indicating the Si/C and Si/porous C composites have higher electric conductivity due to the presence of the nitrogen-rich carbon matrix. After 100 cycles, the interface impedance for the Si/porous C electrode has become lower, which may be ascribed to its stable structure during cycling as well as the activation of the electrodes and the sufficient contact between the activated materials and the electrolyte. On the contrary, the interface impedance of the pure Si electrode and the Si/C electrode has increased after 100 cycles, which is attributed to the electrode pulverization and cracks after cycling caused by the large volume changes of Si nanoparticles during lithiation and delithiation processes. Hence, owing to the nitrogen-rich porous carbon matrix, the Si/porous C composite demonstrates much lower interface impedance compared with the Si/C and the bare nano-Si electrodes, indicating the lower electrochemical reaction resistance during the lithiation/delithiation processes and the stable SEI film formed. These results for the Si/porous C electrode are in good agreement with the above reported excellent electrochemical performance.

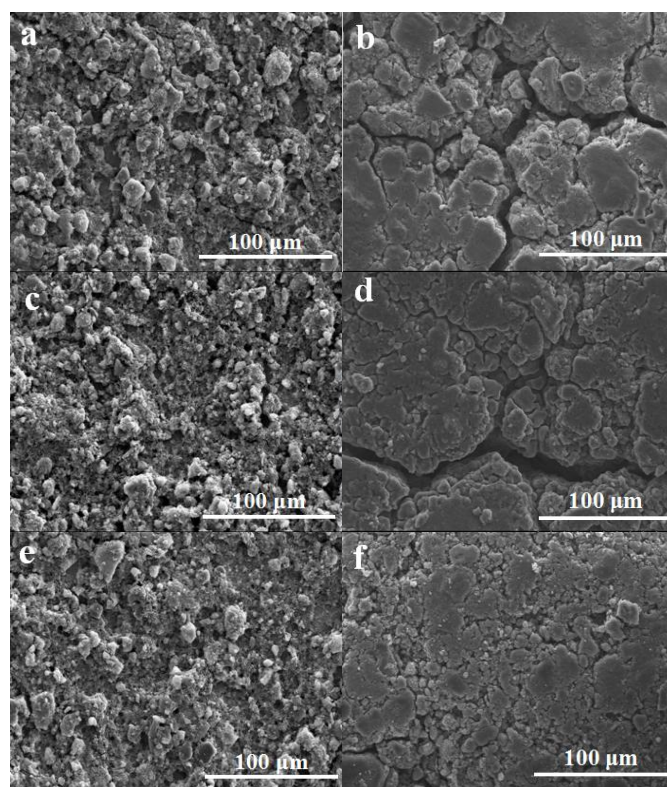


Fig. 9 SEM images of the Si electrode (a), Si/C electrode (c) and Si/porous C electrode (e) before cycling; SEM images of the Si electrode (b), Si/C electrode (d) and Si/porous C electrode (f) after 100 cycles at 100 mA g^{-1} .

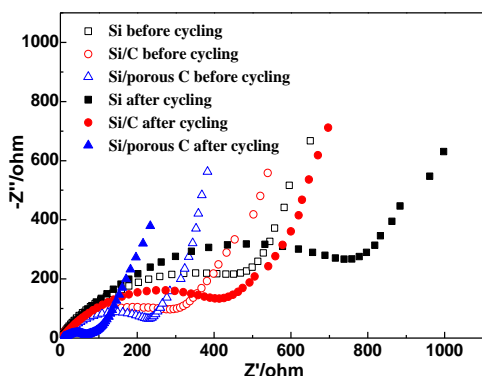


Fig. 10 Nyquist plots of the Si, Si/C and Si/porous C composites before cycling and after 100 cycles.

Conclusions

In summary, the Si/porous C composite has been successfully fabricated by simply adhering the Si nanoparticles to the nitrogen-rich porous carbon framework prepared by using gelatin as the nitrogen-rich carbon precursor and nano-CaCO₃ particles as the template. The nitrogen-rich porous C matrix with high specific surface area, large porosity, excellent conductivity, high resiliency and good mechanical strength can not only ensure the rapid Li⁺ ion transport and improve the electrochemical reaction kinetics but also can provide sufficient space to buffer the volume change of Si nanoparticles during the charging/discharging process. By contrast with the bare Si nanoparticles and the conventional Si/C composite, the Si/porous C composite shows much better electrochemical performance. It exhibits a reversible capacity of 1103 mA h g⁻¹ after 100 cycles at a current density of 100 mA g⁻¹ and 766 mA h g⁻¹ at 2 A g⁻¹, much higher than those of commercial graphite anodes. Besides, the controllable fabrication process is facile, simple and can be easily scaled up. In addition to Si, the new concept for preparing the Si/nitrogen-rich porous C composite can also be applied to other high-capacity anode and cathode materials systems that experience large volume expansion to improve the cycle life.

Acknowledgements

This work was financially supported by the Fund from National High Technology Research and Development Program 863 (no. 2011AA11A256, no. 2012AA052202).

References

- J. B. Goodenough and Y. Kim, *Chem. Mater.*, 2010, **22**, 587.
- M. Armand and J. M. Tarascon, *Nature*, 2008, **451**, 652.
- M. Winter, J. O. Besenhard, M. E. Spahr and P. Novak, *Adv. Mater.*, 1998, **10**, 725.
- N. Liu, H. Wu, M. T. McDowell, Y. Yao, C. M. Wang and Y. Cui, *Nano Lett.*, 2012, **12**, 3315.
- X. H. Liu, L. Zhong, S. Huang, S. X. Mao, T. Zhu and J. Y. Huang, *ACS Nano*, 2012, **6**, 1522.
- L. F. Cui, R. Ruffo, C. K. Chan, H. Peng and Y. Cui, *Nano Lett.*, 2009, **9**, 491.
- L. H. Lin, X. Z. Sun, R. Tao, Z. C. Li, J. Y. Feng and Z. J. Zhang, *J. Appl. Phys.*, 2011, **110**, 7.
- L. Cui, Y. Yang, C. Hsu and Y. Cui, *Nano Lett.*, 2009, **9**, 3370.
- L. F. Cui, L. B. Hu, J. W. Choi and Y. Cui, *ACS Nano*, 2010, **4**, 3671.
- M. H. Park, M. G. Kim, J. Joo, K. Kim, S. Ahn, Y. Cui and J. Chao, *Nano Lett.*, 2009, **9**, 689.
- H. Wu, G. Chan, J. W. Choi, I. Ryu, Y. Yao, M. T. McDowell, S. W. Lee, A. Jackson, Y. Yang, L. Hu and Y. Cui, *Nat. Nanotechnol.*, 2012, **7**, 310.
- L. Ji and X. Zhang, *Carbon*, 2009, **47**, 3219.
- T. H. Hwang, Y. M. Lee, B. S. Kong, J. S. Seo and J. W. Choi, *Nano Lett.*, 2011, **12**, 802.
- Y. Yao, M. T. McDowell, I. Ryu, H. Wu, N. Liu, L. B. Hu, W. D. Nix and Y. Cui, *Nano Lett.*, 2011, **11**, 2949.
- P. R. Abel, Y. M. Lin, H. Celio, A. Heller and C. B. Mullins, *ACS Nano*, 2012, **6**, 2506.
- M. K. Datta, J. Maranchi, S. J. Chung, R. Epur, K. Kadakia, P. Jampani and P. N. Kumta, *Electrochim. Acta*, 2011, **56**, 4717.
- H. P. Jia, P. F. Gao, J. Yang, J. L. Wang, Y. N. Nuli and Z. Yang, *Adv. Energy Mater.*, 2011, **1**, 1036.
- H. C. Tao, L. Z. Fan and X. H. Qu, *Electrochim. Acta*, 2012, **71**, 194.
- H. C. Tao, M. Huang, L. Z. Fan and X. H. Qu, *Electrochim. Acta*, 2013, **89**, 394.
- H. C. Tao, L. Z. Fan, W. L. Song, M. Wu, X. B. He and X. H. Qu, *Nanoscale*, 2014, **6**, 3138.
- M. S. Wang, W. L. Song and L. Z. Fan, *J. Mater. Chem. A*, 2015, **3**, 12709.
- A. Vu, Y. Qian and A. Stein, *Adv. Energy Mater.*, 2012, **2**, 1056.
- H. Kim and J. Cho, *Nano Lett.*, 2008, **8**, 3688.
- Y. H. Xu, Y. J. Zhu and C. S. Wang, *J. Mater. Chem. A*, 2014, **2**, 9751.
- Y. Mao, H. Duan, B. Xu, L. Zhang, Y. S. Hu, C. C. Zhao, Z. X. Wang, L. Q. Chen and Y. S. Yang, *Energy Environ. Sci.*, 2012, **5**, 7950.
- L. Qie, W. M. Chen, Z. H. Wang, Q. G. Shao, X. Li, L. X. Yuan, X. L. Hu, W. X. Zhang and Y. H. Huang, *Adv. Mater.*, 2012, **24**, 2047.
- M. S. Wang and L. Z. Fan, *J. Power Sources*, 2013, **244**, 570.
- L. Yue, W. S. Li, F. Q. Sun, L. Z. Zhao and L. D. Xing, *Carbon*, 2010, **48**, 3079.
- H. S. Zhou, S. M. Zhu, M. Hibino, I. Honma and M. Ichihara, *Adv. Mater.*, 2003, **15**, 2107.
- L. Guo, W. Yoon and B. Kim, *Electron. Mater. Lett.*, 2012, **8**, 405.
- J. C. Guo, X. L. Chen and C. S. Wang, *J. Mater. Chem.*, 2010, **20**, 5035.
- J. T. McCann, B. Lim, R. Ostermann, M. Rycenga, M. Marquez and Y. Xia, *Nano Lett.*, 2007, **7**, 2470.
- Y. P. Wu, S. B. Fang and Y. Y. Jiang, *Solid State Ionics*, 1999, **120**, 117.
- Y. P. Wu, C. Y. Jiang, C. R. Wan, S. B. Fang and Y. Y. Jiang, *J. Appl. Polym. Sci.*, 2000, **77**, 1735.
- F. Kapteijn, J. A. Moulijn, S. Matzner and H. P. Boehm, *Carbon*, 1999, **37**, 1143.
- Z. Y. Jiang, C. L. Li, S. J. Hao, K. Zhu and P. Zhang, *Electrochim. Acta*, 2014, **115**, 393.
- C. K. Chan, H. Peng, G. Liu, X. F. McIlwrath, R. A. Huggins and Y. Cui, *Nat. Nanotechnol.*, 2008, **3**, 31.
- M. Ge, J. Rong, X. Fang and C. Zhou, *Nano Lett.*, 2012, **12**, 2318.
- M. Green, E. Fielder, B. Scrosati, M. Wachtler and J. S. Moreno, *Electrochim. Solid-State Lett.*, 2003, **6**, A75.
- B. Xu, L. Shi, X. W. Guo, L. Peng, Z. X. Wang, S. Chen and G. P. Cao, *Electrochim. Acta*, 2011, **56**, 6464.

- 41 J. Deng, H. Ji, C. Yan, J. Zhang, W. Si, S. Baunack, S. Oswald, Y. Mei and O. Schmidt, *Angew. Chem. Int. Ed.*, 2013, **52**, 2326.
- 42 Y. Zhu, W. Liu, X. Zhang, J. He, J. Chen, Y. Wang and T. Cao, *Langmuir*, 2013, **29**, 744.
- 43 J. Guo, A. Sun, X. Chen, C. Wang and A. Manivannan, *Electrochim. Acta*, 2011, **56**, 3981.
- 44 R. Ruffo, S. S. Hong, C. K. Chan, R. A. Huggins and Y. Cui, *J. Phys. Chem. C*, 2009, **113**, 11390.

A graphical and textual abstract

A novel Si/nitrogen-rich porous carbon composite was prepared by simply using gelatin as nitrogen-rich carbon precursor and nano- CaCO_3 as template.

